Insights into Grain Structures and Their Reactivity on Grade-2 Ti Alloy Surfaces by Scanning Electrochemical Microscopy

Renkang Zhu, Catherine Nowierski, Zhifeng Ding,* James J. Noël, and David W. Shoesmith*

Department of Chemistry, The University of Western Ontario, London, Ontario N6A 5B7, Canada

Received January 4, 2007. Revised Manuscript Received March 11, 2007

The corrosion resistance of titanium and its alloys is a desirable property for many applications in materials science. In this report, the properties of the passive oxide film (TiO_2) were examined by scanning electrochemical microscopy (SECM). A homemade closed-loop scanning electrochemical microscope was used to study these properties at the micrometer scale using ferrocenemethanol (Fc) as the redox mediator. The experimental results showed that the passive properties of a well-polished ASTM Grade-2 titanium (Ti-2) sample differed from region to region as indicated by the different current responses of the ultramicroelectrode (UME) on the SECM images. Selected spots with high feedback tip current were examined more closely by additional scanning. It was concluded that active spots with high positive feedback current were indicative of reactive structures located along crystalline grain boundaries, especially at the triple points. This observation is confirmed by comparing SECM results with optical micrographs reported in the literature. Previous metallographic investigations show these are the sites where the impurity iron content of the alloy congregates. This is confirmed by our experiments on scanning electron microscopy and energy dispersive X-ray analysis. For the first time, grain microstructure maps have been constructed on the SECM images, based on the above active sites. The properties of TiO_2 films on Ti-2 were also assessed at various applied potentials. The reactivity of the oxide-covered Ti-2 surface increased and more active spots appeared when the Ti-2 bias potential was made more negative. This was attributed to oxide reduction (Ti(IV) to Ti(III)) and the onset of the absorption of hydrogen. The potential at which this change occurred varied at different sites on the scale of the grain structure (20−100 μm). These results demonstrate that SECM is a noninvasive analytical methodology that can provide insights into the structures and reactivities of Ti-2.

Introduction

As the rate of worldwide electricity consumption increases, nuclear power becomes an increasingly attractive energy source. As a result, nuclear waste disposal is a rapidly growing challenge for those countries that consume nuclear power. Methods of disposal of nuclear wastes have been under study for more than 20 years, and various geologic formations, supplemented by a series of engineered barriers, to impede radionuclide release to the biosphere[1] have been studied. Within this sequence of barriers, the performance of the metallic container, within which the waste would be sealed prior to emplacement, is extremely important. It would be the only absolute barrier in the system, and its performance can be, at least partially, controlled by choice of fabrication material and design and engineering. Regulatory release limits make it necessary to achieve containment for thousands to tens of thousands of years.

Because of their excellent corrosion resistance,[2−4] titanium alloys are well-studied candidates for the fabrication of engineered barriers under both anodic and cathodic conditions.[5−16] The chemical compositions and mechanical properties of a wide range of titanium alloys are well-

* To whom correspondence should be addressed. E-mail: zfding@uwo.ca.

(1) Shoesmith, D. W. *Corrosion* **2006**, *62*, 703.
(2) He, X. Effects of Temperature, Impurities, and Alloying Elements on the Crevice Corrosion of Alpha Titanium Alloys. Ph.D. Thesis, The University of Western Ontario, London, Canada, 2003.
(3) Donachie, M. J., Jr. *Titanium: A Technical Guide*, 2nd ed.; ASM International: Materials Park, OH, 2000.
(4) Been, J.; Grauman, J. S. In *Uhlig's Corrosion Handbook*, 2nd ed.; Revie, R. W., Ed.; John Wiley and Sons, Inc.: New York, 2000; p 863.
(5) Shoesmith, D. W.; Ikeda, B. M.; LeNeveu, D. M. *Corrosion* **1997**, *53*, 820.
(6) Ikeda, B. M.; Bailey, M. G.; Cann, D. C.; Shoesmith, D. W. *Int. Corros. Conf. Ser.* **1990**, *NACE-9*, 439.
(7) He, X.; Noel, J. J.; Shoesmith, D. W. Effects of temperature and metallurgical features on crevice corrosion of titanium grade-2; Aerospace Materials: Developments, Durability, Testing and Life Cycle Issues. Presented at the International Symposium on Aerospace Materials: Developments, Durability, Testing and Life Cycle Issues, Montreal, QC, Canada, Aug 11−14, 2002.
(8) He, X.; Noel, J. J.; Shoesmith, D. W. *J. Electrochem. Soc.* **2002**, *149*, B440.
(9) He, X.; Noel, J. J.; Shoesmith, D. W. Effects of iron content on microstructure and crevice corrosion of titanium Grade-2; Environmental Degradation of Materials and Corrosion Control in Metals. Presented at the 2nd International Symposium on Environmental Degradation of Materials and Corrosion Control in Metals, Vancouver, BC, Canada, Aug 24−27, 2003.
(10) He, X.; Noel, J. J.; Shoesmith, D. W. *Corrosion* **2004**, *60*, 378.
(11) He, X.; Noel, J. J.; Shoesmith, D. W. *Corros. Sci.* **2005**, *47*, 1177.
(12) Shoesmith, D. W.; Noel, J. J.; Hardie, D.; Ikeda, B. M. *Corros. Rev.* **2000**, *18*, 331.
(13) Nakayama, G.; Fukuya, Y.; Akashi, M.; Sawa, S.; Kanno, T.; Owada, H.; Otsuki, A.; Aasano, H. Hydrogen-induced Stress Corrosion Crack Initiation and Propagation in Titanium Alloys in Deep Underground Environments. In *Prediction of Long term Corrosion behaviour in Nuclear Waste Systems* Andra, Chattenay-Malabry, France, 2004; pp 35.
(14) *BSC. Hydrogen-Induced Cracking of the Drip Shield*, ANL-EBS-MD-000006 REV 02, Bechtel SAIC Company: Las Vegas, NV, 2004.

10.1021/cm070023d CCC: $37.00
Published on Web 04/24/2007

known,[17] and the properties of the alloys relevant to waste management applications have been summarized.[16] Titanium spontaneously reacts in air and aqueous solutions to form a chemically inert and tightly adherent oxide, which confers passivity on the metal (or alloy). This oxide may be amorphous or crystalline, depending on the conditions of growth. Thus, Raman spectroscopy has indicated amorphicity over a wide range of applied potentials,[18] although the results of electron diffraction and photoelectrochemical measurements have been interpreted to indicate the presence of a rutile structure.[19] Films grown at higher temperatures (e.g., 60 °C) commonly contain anatase, the slightly less stable form of TiO_2.[19,20]

Ti ions in TiO_2 have a $Ti^{4+}(3d^0)$ electron configuration, making the oxide an insulator, or a wide band semiconductor with a band gap of 3.05 eV. Deviations from stoichiometry (TiO_{2-x}) give the thin oxide film n-type semiconductor characteristics,[21] due to the presence of a combination of oxygen vacancies and interstitial Ti^{3+} ions, which lead to the trapping of electrons in a band just below the conduction band edge.[22] The presence of defects in the native oxide (grown on natural exposure, first to the air, then to an aqueous environment) is clearly demonstrated by the higher density of states at energies corresponding to what would be the band gap in crystalline rutile or anodically grown films.[23]

On the basis of micro-ellipsometry and photocurrent scanning techniques, Schultze and co-workers[24,25] showed that the properties of the passive oxide depend on crystallographic texture, that is, the thickness and electronic properties of the film change from grain to grain depending on its orientation. Given these changes, structural mismatches in grain boundaries are inevitable. In addition, the grain size of commercial Ti-2 is known to be controlled by the unavoidable impurity, Fe. When the Fe content is low, Fe accumulates in the grain boundaries but does not impede grain growth, and α-phase grain sizes in excess of 1 mm in dimension are possible. When the Fe content is higher, Fe-containing β-phase is stabilized along the α grain boundaries, blocking their growth and resulting in a finer grained material.[10] For sufficiently high Fe content, Watanabe et al.[26] have shown that the formation of Ti_xFe intermetallic precipitates can occur, particularly at the triple points. That the presence of Fe may destabilize the oxide at/over grain boundaries is suggested by the potentiostatic experiments of Curty and Virtanen in NaCl and NaBr solutions.[27] They observed small current transients, associated with film breakdown/repair events, on commercially pure Ti (Ti-2) but not on high purity titanium (99.99%).

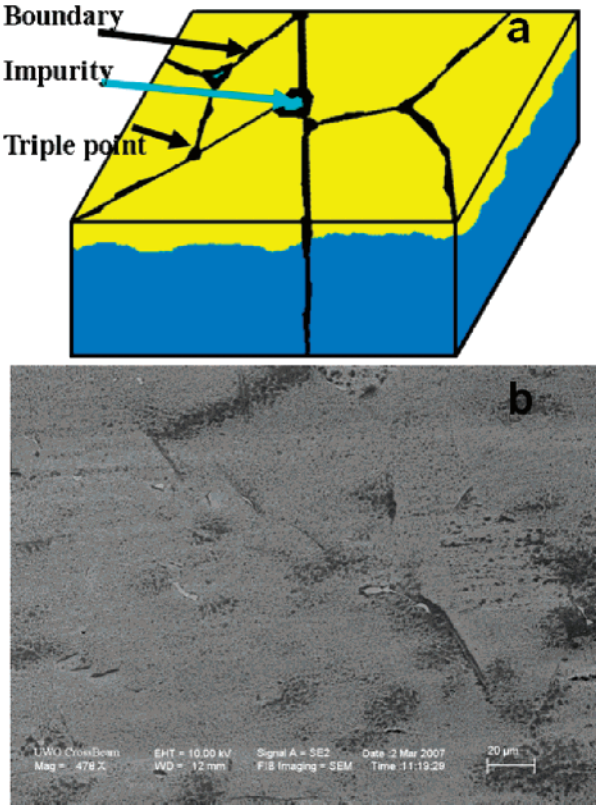

Figure 1. (a) Illustration of the surface structures of Grade-2 titanium (Ti-2). Ti-2 is made of crystalline α-grains (blue), with grain boundaries between them (black lines). Points where three grains meet are termed triple points (light blue). The oxide film (yellow) always covers the Ti-2 surface. Impurities are possibly accumulated at the boundaries and/or triple points. (b) Typical image of Ti-2 by SEM.

The role of Fe impurities leading to the accumulation of corrosion damage on Ti-2, by crevice corrosion (CC) and hydrogen absorption leading to hydrogen-induced cracking (HIC), is known but generally unexplained.[10] It has been shown that oxide film breakdown leading to initiation of CC occurs more rapidly at higher Fe content,[2] but studies of the influence of Fe on hydrogen absorption yielded conflicting results.[10]

Because Fe is associated with the grain boundaries in these materials, an investigation of grain boundary properties is important in determining the quality of the passive film on Ti alloys. If Fe is associated with flaws in the film, then these are likely locations for the onset of corrosion processes known to lead to failure of Ti engineered structures.[2] Figure 1a illustrates the grain boundaries and triple points in Ti-2 based on the optical micrograph of the material used in this work, shown in Figure S3 of Supporting Information. The grain size varies over the wide range of 20−100 μm.

(15) *BSC. General Corrosion and Localized Corrosion of the Drip Shield*, ANL-EBS-MD-000004 REV 02; Bechtel SAIC Company: Las Vegas, NV, 2004.
(16) Hua, F.; Mon, K.; Pasupathi, P.; Gordon, G.; Shoesmith, D. *Corrosion* **2005**, *61*, 987.
(17) ASTM B 265-02. Standard Specification for Titanium and Titanium Alloy Strip, Sheet and Plate; ASTM International: West Conshohocken, PA, 2002.
(18) Shibata, T.; Zhu, Y.-C. *Corros. Sci.* **1995**, *37*, 253.
(19) Tyler, P. S.; Kozlowski, M. R.; Smyrl, W. H.; Akanasoski, R. T. *J. Electroanal. Chem.* **1987**, *237*, 295.
(20) Shibata, T.; Zhu, Y.-C. *Corros. Sci.* **1994**, *36*, 1735.
(21) Torresi, R. M.; Camara, O. R.; de Pauli, C. P.; Giordano, M. C. *Electrochim. Acta* **1987**, *32*, 1291.
(22) Jarzebski, Z. M. *Oxide Semiconductors*; Pergamon Press: Oxford, New York, 1973; Vol. 4.
(23) Casillas, N. Characterization of precursor sites for pitting corrosion on titanium. Ph.D. Thesis, University of Minnesota, 1993.
(24) Michaelis, A.; Kudelka, S.; Schultze, J. W. *Electrochim. Acta* **1998**, *43*, 119.
(25) Schultze, J. W.; Schweinsberg, M. *Electrochim. Acta* **1998**, *43*, 2761.
(26) Watanabe, T.; Shindo, T.; Naito, H. Effect of iron content on the breakdown potential for pitting of titanium in NaCl solutions. Presented at the Sixth World Conference on Titanium, Cannes, France, 1988.
(27) Curty, C.; Virtanen, S. Presented at the Electrochemical Society Symposium on Passivity and Localized Corrosion, Honolulu, Hawaii, U.S.A., Oct 17−22, 1999.

The presence of Fe in Ti is known to inhibit grain growth, and grain sizes in excess of iron are commonly observed for Fe contents in the range of 0.04 wt % compared to the 0.078 wt % present in our material.[2] The smaller grain size and the wide distribution of grain sizes in our material are consistent with the inhomogeneous presence of Fe in the grain boundaries. That Fe is present at these locations is demonstrated by scanning electron microscopy (SEM)/energy dispersive X-ray (EDX) analyses. Figure 1b shows a typical SEM image of a polished specimen, and EDX analyses at grain boundary locations indicate Fe contents in the range ~5−17% (Table S1 in Supporting Information).

Scanning electrochemical microscopy (SECM) is useful in the investigation of grain boundary properties, because it can supply in situ electrochemical information at high spatial resolution (micrometer scale). SECM[28] can determine the chemical and biochemical kinetics,[29−32] image local chemical activities,[33−43] and fabricate micrometer scale structures.[44−46] The most significant advantage of SECM is its capability to probe chemical information concerning electron and ion transfer processes at the interfaces between substrates and their contacting electrolyte solutions. Normally, an ultramicroelectrode (UME), a microscale disk-shaped platinum, gold or carbon electrode insulated in a glass sheath, is used as the SECM probe (tip). A constant potential is applied to the SECM probe to run a fast electrochemical reaction of one redox species (the mediator). The electrochemical current is determined by hemispherical diffusion of the reactant to the electrode surface from the bulk solution. When the biased probe approaches a substrate, this current is perturbed by the substrate at close proximity through either blockage of the diffusion (on an insulator, negative feedback) or dominant regeneration of the reacted species from the substrate (on a conductor, positive feedback).[28] It is possible to image the surface topography and/or chemical reactions on the surface by detecting the current perturbation when the tip is rastered in a plane close to the substrate.

Casillas et al.[47,48] used SECM to study the breakdown of native and anodically grown oxide films on commercially pure Ti electrodes in bromide solution. Basame and White[49] studied these highly localized electrochemical activities on pure Ti with different redox media (iodide, bromide, and ferrocyanide) using SECM and other electrochemical methods. The surface density of the electroactive sites for their Ti sample was found to be about 20 ± 5 sites/cm^2, with sites having a diameter of about 50 μm. The same authors measured the current density at microscopic redox-active sites on pure Ti.[50] Other research in this area[50−57] has focused on the corrosion of Ti biased to positive potentials. Although these authors used Ti samples covered by a native oxide film, the oxide film thickness changed with the applied positive bias potential at a rate of 2.5 nm/V.[49,58] While instructive in defining potential pitting breakdown sites at positive applied potentials (>1 V vs SCE), these studies did not probe the properties of passive Ti at the micrometer scale necessary to determine grain boundary properties.

In this work, the surface structures and interfacial electrochemical reactions of Ti-2 were studied by SECM and other related electrochemical methods. Ferrocenemethanol (Fc) was used as the redox mediator. Because the electrochemical reaction of Fc on the SECM probe is very fast, interactions of this mediator with the Ti-2 substrate (feedback) are the determinant reaction step. The SECM feedback current yields, therefore, chemical information concerning the surface of Ti-2, in terms of Ti composition, structure, formation, dissolution, and reactivity. In this way, active and passive spots were determined. For the first time, grain structure maps were constructed based on SECM images. The spatial- and potential-dependent structures and behaviors were assessed.

Experimental Section

Chemicals. Fc (97%, Aldrich, Mississauga, Canada) was prepared at a concentration of 0.9 mmol/L with 0.1 mol/L sodium chloride (NaCl, ACS reagent, >99%, Aldrich) or potassium chloride (KCl, ACS reagent, 99+%, Aldrich) as supporting electrolyte. Deionized water (Milli-Q, Millipore, 18.2 MΩ·cm resistivity) was used to prepare all aqueous solutions.

(28) Bard, A. J. In *Scanning Electrochemical Microscopy*; Bard, A. J., Mirkin, M. V., Eds.; Marcel Dekker: New York, 2001; p 1.
(29) Ding, Z.; Quinn, B. M.; Bard, A. J. *J. Phys. Chem. B* **2001**, *105*, 6367.
(30) Amemiya, S.; Ding, Z.; Zhou, J.; Bard, A. J. *J. Electroanal. Chem.* **2000**, *483*, 7.
(31) Fonseca, S. M.; Barker, A. L.; Ahmed, S.; Kemp, T. J.; Unwin, P. R. *Chem. Commun.* **2003**, 1002.
(32) Katemann, B. B.; Inchauspe, C. G.; Castro, P. A.; Schulte, A.; Calvo, E. J.; Schuhmann, W. *Electrochim. Acta* **2003**, *48*, 1115.
(33) Fan, F.-R. F. SECM imaging. In *Scanning Electrochemical Microscopy*; Bard, A. J., Mirkin, M. V., Eds.; Marcel Dekker: New York, 2001; p 111.
(34) Liu, B.; Rotenberg, S. A.; Mirkin, M. V. *Anal. Chem.* **2002**, *74*, 6340.
(35) MacPerson, J. V.; Jones, C. E.; Barker, A. L.; Unwin, P. R. *Anal. Chem.* **2002**, *74*, 1841.
(36) Mauzeroll, J.; Bard, A. J. *Proc. Natl. Acad. Sci. U.S.A.* **2004**, *101*, 7862.
(37) Tsionsky, M.; Cardon, Z. G.; Bard, A. J.; Jackson, R. B. *Plant Physiol.* **1997**, *113*, 895.
(38) Yasukawa, T.; Kaya, T.; Matsue, T. *Electroanalysis* **2000**, *12*, 653.
(39) Zhao, C.; Sinha, J. K.; Wijayawardhana, C. A.; Wittstock, G. *J. Electroanal. Chem.* **2004**, *561*, 83.
(40) Turcu, F.; Schulte, A.; Hartwich, G.; Schuhmann, W. *Angew. Chem., Int. Ed.* **2004**, *43*, 3482.
(41) Fernandez, J. L.; Mano, N.; Heller, A.; Bard, A. J. *Angew. Chem., Int. Ed.* **2004**, *43*, 6355.
(42) Zhu, R.; Ding, Z. *Can. J. Chem.* **2005**, *83*, 1779.
(43) Zhu, R.; Macfie, S. M.; Ding, Z. *J. Exp. Bot.* **2005**, *56*, 2831.
(44) El-Giar, E. M.; Said, R. A.; Bridges, G. E.; Thomson, D. J. *J. Electrochem. Soc.* **2000**, *147*, 586.
(45) Wittstock, G. *Fresenius' J. Anal. Chem.* **2001**, *370*, 303.
(46) Katemann, B. B.; Schulte, A.; Schuhmann, W. *Chem.—Eur. J.* **2003**, *9*, 2025.
(47) Casillas, N.; Charlebois, S. J.; Smyrl, W. H.; White, H. S. *J. Electrochem. Soc.* **1993**, *140*, L142.
(48) Casillas, N.; Charlebois, S.; Smyrl, W. H.; White, H. S. *J. Electrochem. Soc.* **1994**, *141*, 636.
(49) Basame, S. B.; White, H. S. *J. Phys. Chem.* **1995**, *99*, 16430.
(50) Basame, S. B.; White, H. S. *J. Phys. Chem. B* **1998**, *102*, 9812.
(51) Basame, S. B.; White, H. S. *Book of Abstracts, 214th ACS National Meeting, Las Vegas, NV, September 7−11*; American Chemical Society: Washington, DC, 1997; ANYL.
(52) Basame, S. B.; White, H. S. *Proc. Electrochem. Soc.* **1999**, *99-5*, 15.
(53) Basame, S. B.; White, H. S. *Anal. Chem.* **1999**, *71*, 3166.
(54) Fusimi, K.; Okawa, T.; Seo, M. *Electrochemistry (Tokyo)* **2000**, *68*, 950.
(55) Garfias-Mesias, L. F.; Alodan, M.; James, P. I.; Smyrl, W. H. *J. Electrochem. Soc.* **1998**, *145*, 2005.
(56) Garfias-Mesias, L. F.; James, P. I.; Smyrl, W. H. *Proc. Electrochem. Soc.* **1997**, *97-7*, 247.
(57) James, P.; Casillas, N.; Smyrl, W. H. *Proc. Electrochem. Soc.* **1996**, *95-15*, 425.
(58) Marsh, J.; Gorse, D. *Electrochim. Acta* **1997**, *43*, 659.

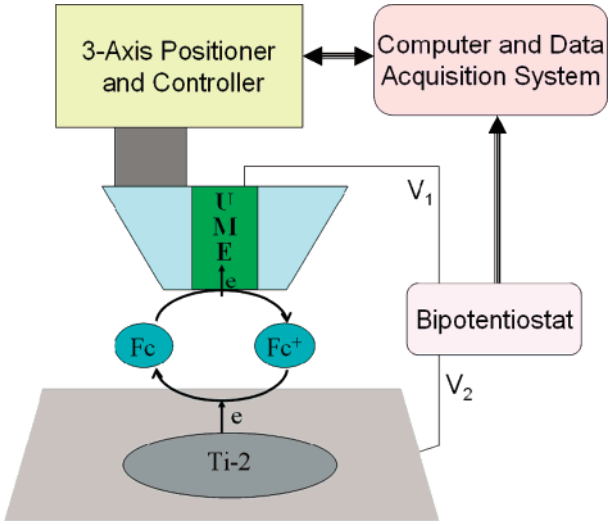

Figure 2. Schematic illustration of the SECM experiments. The Ti-2 sample was clamped between two blocks of Teflon to compose the SECM cell. A bipotentiostat was used in our experiments to bias the potentials of both the CUME and Ti-2 sample simultaneously. Fc, the redox mediator, was oxidized on the CUME tip to generate Fc^+, and the Fc^+ diffused to the Ti-2 surface. If Fc^+ was reduced to Fc at some spots on the substrate surface, the tip current increased so that a positive feedback current was detected by the CUME. These spots were called "active spots". In contrast, the insulating TiO_2 film blocked the Fc diffusion to the UME so that a negative feedback current was observed. The TiO_2 film showed properties of an insulator; such spots were called "nonactive spots".

UME Fabrication. The fabrication of the carbon fiber UME (CUME) has been previously reported.[59] We have modified the procedure as we described for making Pt UMEs elsewhere.[42,43] Our fabrication procedure is described in the Supporting Information.

Characterization of CUMEs for SECM Probes. Normally, three methods were used to characterize the CUMEs as shown in Supporting Information: microscopic videograph; cyclic voltammetry; and probe approach curves (PACs) to a glass substrate.

SECM Instrumentation. The detailed information about our custom-built SECM instrument has been published elsewhere.[42] As illustrated by Figure 2, it consisted of three major components: the electrochemical system (electrochemical analyzer, CH 832A, CH Instruments, Austin, TX); the closed-loop positioning system (FREEDOM 1500-3 Nano Robot system, EXFO Burleigh Products Group, Inc., Canada); and the active data acquisition system consisting of a computer loaded with homemade virtual instruments (VIs) programmed in LabVIEW (Version 7, National Instruments, Austin, TX), a general purpose interface bus (GPIB) board (PCI-GPIB, National Instruments) to communicate with the 8200 controller, and a 16-bit DAQ card (PCI-6052E, National Instruments) with a connection board (BNC-2090, National Instruments). The electrochemical and positioning systems were built together in a Faraday cage to isolate external electrical noise. The constant-height mode was used for imaging where the CUME current was recorded versus lateral coordinates at a fixed height in the vicinity of the Ti-2 sample. All the experiments were performed at room temperature. In general, it took 5 min to finish each 128 × 128 pixel image. The data were displayed *in real time*. A spreadsheet file was saved after each experiment for further analysis.

Ti-2 Sample Preparation and SECM Experiments. Prior to each experiment, the Ti-2 surface was mechanically polished with wet silicon carbide paper (Buehler, Ltd.) in the sequence of 320, 500, 800, 1000, and 1200 grit and then rinsed with copious deionized water. The surface was then polished with 0.3 μm and 0.005 μm alumina powder suspensions, respectively, rinsed with excess amounts of deionized water, and left to air-dry. Thus, the surface of the Ti-2 sample was covered with a thin native layer of titanium oxide film.[60] This sample was clamped between two pieces of Teflon in the electrochemical cell specifically designed for our homemade SECM.[42] The area of the Ti-2 sample exposed to the solution was about 0.50 cm^2. The whole electrochemical cell was mounted on the platform of our SECM setup. Potentials could be applied to both the CUME and the Ti-2 sample (Figure 2) using the electrochemical analyzer (CHI-832A).

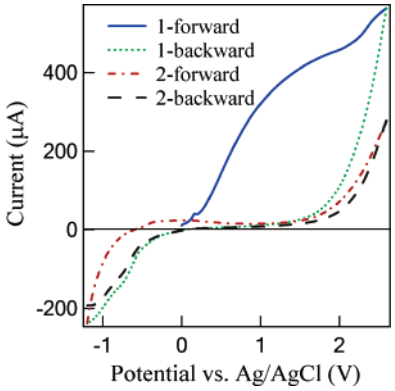

Figure 3. Consecutive CVs of a Ti-2 sample with a surface area of 0.50 cm^2 in 0.1 mol/L NaCl solution. The initial potential was 0.00 V, and the potential range was −1.20 to 2.60 V. The potential sweep rate was 100 mV/s.

SEM and EDX Analysis. SEM imaging, EDX analysis, and EDX mapping were carried on an electron microscope (Leo 1540 FIB/SEM with CrossBeam, Zeiss Nano Technology Systems Division, Germany)

Results and Discussion

CVs of the Ti-2 Sample. A well-polished Ti-2 sample was clamped into the SECM cell containing only 0.1 M NaCl, and a cyclic voltammogram (CV) was recorded at 100 mV/s (Figure 3) using a KCl-saturated Ag/AgCl reference electrode and a Pt counter electrode. On the first scan, the current increased substantially beyond 0.2 V as electric field-assisted growth of an anodic oxide occurred. The increase in current with potential is consistent with previous observations with oxide growth occurring at a rate of 2−2.5 nm/V.[49,58,61,62] At the scan rate used, it is likely that the oxide was amorphous and highly defective.[62] On the reverse scan, the anodic current immediately fell as the field in the oxide was reduced to a value too low to sustain field-assisted oxide growth. For potentials ≤ 0.00 V versus Ag/AgCl, cathodic processes were observed. The decreasing current (an increase of the absolute current value) at more negative potentials is attributed to the reduction of Ti^{IV} to Ti^{III} within the insoluble oxide (at the neutral pH used) and the co-absorption of hydrogen. On the basis of capacitance measurements and charge calculations, Ohtsuka et al.[63] calculated that one atom of H was absorbed for each Ti^{IV} atom reduced, indicating the overall film conversion reaction:

(59) Wightman, R. M.; Wipf, D. O. In *Electroanalytical Chemistry*; Bard, A. J., Ed.; Marcel Dekker: New York, 1988; Vol. 15; p 267.
(60) Andreeva, V. V. *Corrosion* **1964**, *20*, 35t.
(61) Ohtsuka, T.; Masuda, M.; Sato, N. *J. Electrochem. Soc.* **1985**, *132*, 787.
(62) McAleer, J. F.; Peter, L. M. *Faraday Discuss.* **1980**, *70*, 67.
(63) Ohtsuka, T.; Masuda, M.; Sato, N. *J. Electrochem. Soc.* **1987**, *134*, 2406.

$$TiO_2 + xH^+ + xe^- \rightarrow TiO_{2-x}(OH)_x \quad (1)$$

It is this process which is thought to render the oxide permeable to H, thereby allowing the H absorption into the underlying Ti (the first step toward HIC) observed in long-term potentiostatic experiments.[64,65] For polarizations to potentials in the region of −1 V, the increase in current is attributable to H_2 evolution[21] and the rate of H absorption into the metal is markedly increased.[65] For polarizations of sufficient duration a TiH_x layer is formed on the Ti surface.[65,66]

On the second scan (starting from −1.20 V), some of the H absorbed in the oxide was anodically reoxidized, commencing around −0.50 V.[63] For potentials up to ∼1.50 V, no significant anodic current was observed because the field in the existing oxide was insufficient to drive oxide growth. The current increase at higher potentials is attributed to chloride oxidation,

$$2Cl^- \rightarrow Cl_2 + 2e \quad (E_{Cl_2/Cl^-}{}^0 = 1.360\ V)^{61} \quad (2)$$

occurring at the conductive defects in the TiO_2 detected by Casillas et al.,[47,48] Basame and White[49−53,67] and others,[54−57] which leads to pitting in Br^- solutions. Some anodic oxidation of water,

$$H_2O \rightarrow O_2 + 4H^+ + 4e \quad (E_{O_2/H_2O}{}^0 = 1.226)^{61} \quad (3)$$

may also be possible. Additional scans were identical to the second scan.

PACs to the Ti-2 Sample. Because Ti-2 is covered with an oxide with a band gap of about 3.0 eV,[62,63] it should be nonconductive. Negative feedback is expected when the SECM probe is approached to the Ti-2 surface. Figure 4 shows a typical PAC for a CUME, with an RG (the ratio of the total radius of the tip to the radius of the carbon fiber) value of 5.0. The experimental curve fits well to the theoretical curve for negative feedback (RG of 5.1),[68] demonstrating the expected insulating properties of the oxide-covered surface.

From such PACs, the distance between the tip and the Ti-2 sample can be determined from the normalized current superimposed onto the theoretical PAC; for example, in Figure 4 the approach distance was 2.7 μm when the normalized current reached 0.5. Note that it is important to keep similar RG values for SECM UMEs, especially in the negative feedback case.[28] On the other hand, the distance between the tip and the substrate cannot be too small, in case the substrate is tilted. With too small a distance or too large an RG, UME tips can easily scratch the Ti-2 surface, leading to breakage of the tip or substrate surface damage. From our experience, for a CUME with 3.4-μm radius and RG = 5.0, the tip-to-substrate distance should be kept at

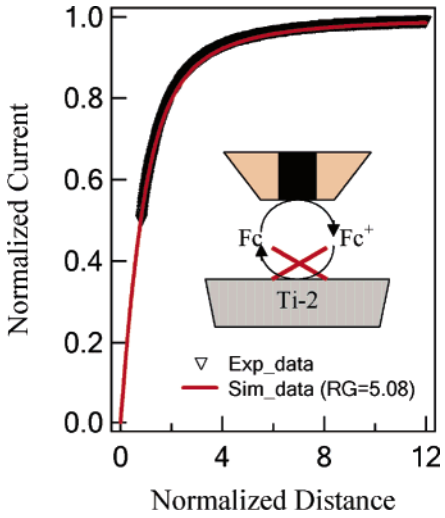

Figure 4. Representative SECM approach curve at the Ti-2 sample surface (triangles) at 1.0 μm/s in 0.9 mmol/L Fc solution with 0.1 mol/L NaCl as the supporting electrolyte. The Ti-2 sample was at its open circuit potential. The CUME had a radius of 3.4 μm with a RG of 5. The potential bias on the CUME was 0.40 V vs Ag/AgCl. The experimental curve fits well with the simulated curve (red line, RG = 5.09), which means that the reverse reaction, the reduction of ferroceniummethanol (Fc+) to Fc on the Ti-2, did not happen (shown in the inset).

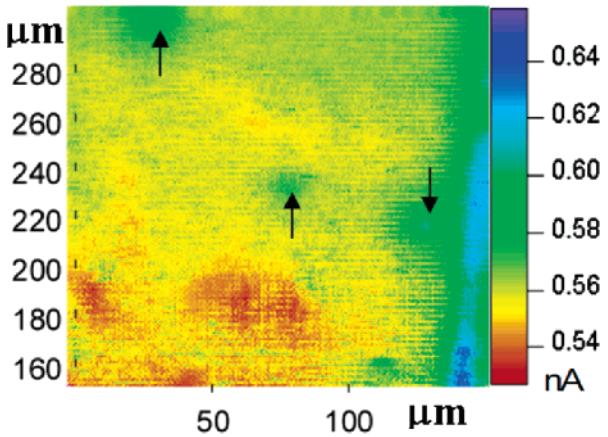

Figure 5. Typical SECM image of the Ti-2 sample without bias potential in 0.9 mol/L Fc solution with 0.1 mol/L NaCl as the supporting electrolyte. The image area is 150 μm × 150 μm with 128 × 128 pixels. The current range was 0.53−0.66 nA. The spots labeled by arrows yielded higher currents than their surroundings.

2.7 μm. At this distance, the scanning lateral range reaches 200 μm × 200 μm without any problem.

Surface Reactivity Detected by SECM Imaging. At a constant height of 2.7 μm, the SECM UME was rastered in the *X*, *Y* plane above the Ti-2 surface without bias potential using the closed-loop positioning system, and the tip currents versus the lateral tip positions were recorded to obtain SECM images. Figure 5 shows a typical SECM image of an unpolarized Ti-2 surface. The tip current range for this image is 0.53−0.66 nA. The gap distance range, 3.8−5.6 μm, was read from a theoretical negative feedback PAC (Figure 4), assuming that the Ti-2 specimen was covered by an oxide layer. Therefore, the roughness of the Ti-2 surface was estimated to be a maximum of 1.8 μm according to the SECM image.[69] Actually, the surface roughness was less than this because the sample surface was slightly tilted. Some spots with a higher current than their surroundings can be

(64) Murai, T.; Ishikawa, M.; Miura, C. *Boshoku Gijutsu* **1977**, *26*, 177.
(65) Shimogori, K. *Corros. Eng. (Japan)* **1981**, *30*, 349.
(66) Noel, J. J.; Bailey, M. G.; Crosthwaite, J. P.; Ikeda, B. M.; Ryan, S. R.; Shoesmith, D. W. Report AECL; Atomic Energy of Canada Limited: Pinawa, Manitoba, 1996; AECL11608.
(67) Basame, S. B.; White, H. S. *Langmuir* **1999**, *15*, 819.
(68) Shao, Y.; Mirkin, M. V. *J. Phys. Chem. B* **1998**, *102*, 9915.

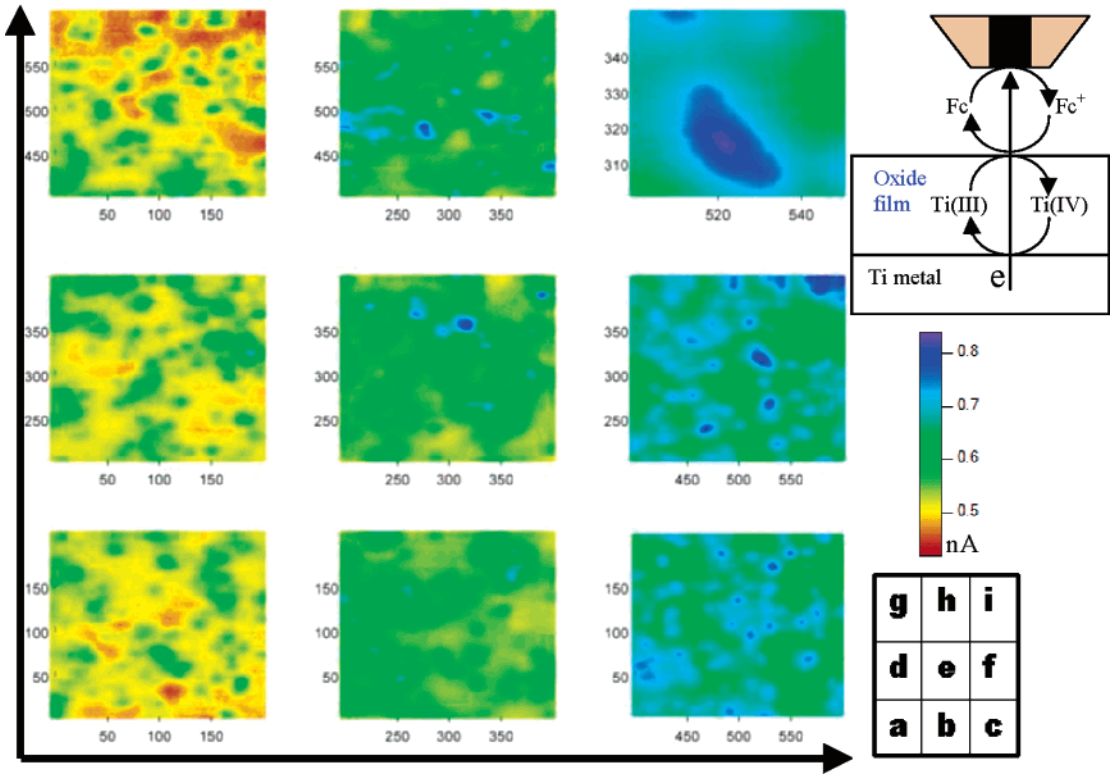

Figure 6. Typical SECM images of the Ti-2 sample surface in 0.9 mmol/L Fc solution with 0.1 mmol/L NaCl as the supporting electrolyte. The total scan area is 600 μm × 600 μm, which was divided into nine images, of which eight images are shown (a−h). The current scale bar (from 0.42 to 0.84 nA) for each image is displayed on the right. The tip current in bulk solution was 0.90 nA. Image i is the magnified image of an active spot in image f. The potential on the substrate was held at 0.00 V vs Ag/AgCl. Other experimental conditions were the same as those described in Figure 5.

observed in this image as labeled with the arrows shown in Figure 5. On approach of the CUME toward these spots a typical negative feedback PAC was observed. These results demonstrate that the current differences in Figure 5 can be attributed to topography changes and not changes in reactivity on the sample surface. From the theoretical curve shown in Figure 4, the depth of the three holes was estimated to be about 0.4 μm (the current difference was about 0.029 nA) lower than their surroundings.

When a potential of 0.00 V versus Ag/AgCl was applied to the Ti-2 sample, a total area of 600 μm × 600 μm was surveyed to search for current changes on the surface. To avoid damaging the CUME, nine images, each with a surface area of 200 μm × 200 μm, were recorded consecutively instead of one large area image (Figure 6). These images were clearly different from that in Figure 5, with many high current spots (blue spots, termed as active spots), up to 0.84 nA, visible in the images. These spots were not visible with no applied potential on the Ti-2 sample. A PAC toward the blue spotted areas (Figure S2 in Supporting Information) showed that the high current was caused by positive feedback from the surface; that is, Fc^+ generated at the SECM tip was reduced back to Fc on diffusing to these active spots:

$$Fc^+ + e^- \rightarrow Fc \quad \text{(on the substrate)} \qquad (4)$$

This recycling reaction is shown in the inset of Figure 6. Clearly, the Ti-2 surface covered with the native oxide film was not homogeneous, and the reactivity on the surface varied from region to region.

Table 1. Characteristics of Active Spots on the Ti-2

	scan area (μm^2)	number	diameter range (μm)	density (spots/mm^2)	area coverage (%)
1	600 × 600	141	2−17	392	10
2	100 × 100	5	4−14	500	12
3	200 × 200	13	3−17	325	10
average				388	10

We zoomed in on some of the high current spots to determine their size, as shown in Figure 6i. The current difference between the most reactive spot and its surroundings was about 0.21 nA. This difference was much higher than that for the spots labeled in Figure 5 and was not only due to a topographical difference but also due to partial positive feedback from the Ti-2 surface. Comparison of PACs taken at these active spots and those from the background confirms this conclusion (Figure S2, Supporting Information). The number, density, and fractional coverage of the high current spots on the scanned area were estimated and are shown in Table 1.

These active spots can be distinguished from those observed by the groups of White and Smyrl[47−49,51,55,56] by a number of features: (1) White's and Smyrl's active spots were observed in bromide solutions and only at positive potentials in the range of 1 V or greater; (2) their active spot density of 30 sites/cm^2 was much less than what we observed (Table 1); and (3) the diameter of their active spots was between 10 and 50 μm, making them considerably larger than the ones observed in this work. They attributed the

(69) Wei, C.; Bard, A. J. *J. Electrochem. Soc.* **1995**, *142*, 2523.

observation of active spots to the presence of impurities but did not succeed in identifying their nature or composition.

The primary impurity in our Ti-2 is Fe, which, as discussed, resides primarily in the grain boundaries of the sample (Table S1 and Figure S5 in Supporting Information). Inspection of the photomicrograph of the metallographically etched surface, Figure S3 (Supporting Information), clearly showed the grain boundaries and the large number of triple points.[2] Because the grain boundary volume is greatest at these latter locations, we expect the highest accumulation of defects and the highest concentrations of Fe impurity at these sites. Hence, we propose that the most active spots observed on the SECM images were the triple points and, to a slightly lesser degree, the grain boundaries. Thus, the images shown in Figure 6 appear to directly map the grain boundary structure of the substrate Ti-2.

Grain Boundary and Grain Structures. To further demonstrate our point we have joined, by black lines, the high current blue spots observed in two SECM images (200 μm × 200 μm) of the Ti-2 specimen, Figure 7, mapped at a potential of 0.00 V in such a way that two neighboring spots with high current were connected to each other. If we are correct, these lines delineate the grain boundaries and triple points. Comparison of these patterns to our metallograph (Figure S3, Supporting Information)[2] and other published metallographs[65] shows the enclosed areas in the SECM images are on the same size scale as the grains in the micrograph, and the frequency of proposed triple points, defined by the high current blue spots, is very close to that observed in the micrograph. The enclosed areas would be the TiO_2-covered Ti grains.

Of particular interest to us is the behavior of the passive film under cathodic polarization, particularly in the range 0.00 V to −0.50 V, Figure 3. As discussed above, the oxide-covered surface eventually becomes permeable to hydrogen allowing H absorption into the underlying Ti. To date, it has been presumed that this can only happen when oxide reduction (Ti^{IV} to Ti^{III}), accompanied by H absorption into the oxide, occurs. However, the question has been raised as to whether impurities such as Fe, present as intermetallic precipitates and/or Fe-containing β-phase, could act as "windows" in the oxide, thereby allowing H absorption to "bypass" the oxide.[70] Our ability to detect sites in the oxide with enhanced reactivity and to correlate locations with triple points and grain boundaries suggests such "windows" may exist.

The discovery of grain structures on the SECM images can then be further facilitated by varying the applied potential on the Ti-2. Figure 8 shows a series of images taken on the same area of Ti-2 as its potential was changed from −0.05 V to −0.40 V. Figure 8a shows only one active spot (indicated by the arrow) at an applied potential of −0.05 V. That this spot was active was confirmed by a PAC, which showed partial positive feedback (Figure S2, Supporting Information). When the potential was decreased to −0.10 V, two new active spots appeared, Figure 8b,

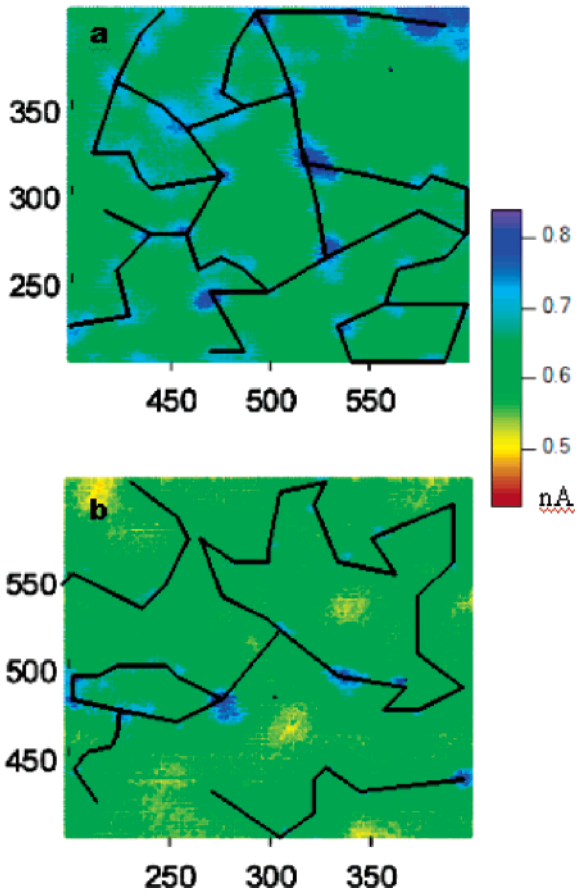

Figure 7. SECM images with possible grain boundary structures on the Ti-2 surface. All the experimental parameters were the same as those described in Figure 6. The current scale in these two images is 0.42−0.84 nA. The tip current in bulk solution was 0.90 nA. The blue spots are the active spots that appeared at the grain boundaries and triple points. The black lines were drawn by connecting the active spots, which represent the grain boundaries on the Ti-2 surface.

connected by a line, suggesting they were associated with a grain boundary. From the general color of the image, it is clear that the current is generally larger at −0.10 V compared to −0.05 V. A further decrease in potential to −0.15 V, Figure 8c, activated additional spots, and their connection suggests that the original active spot in Figure 8a was located at a triple point. Further decreases in potential to −0.40 V led to enhanced activation of the triple point and grain boundaries and also to a general increase in current on the surface of the grains. One complete grain appears to have been outlined once the potential was decreased to the range −0.35 V to −0.40 V.

At potentials below −0.40 V, the oxide film became successively more conductive as a result of reduction reaction 1. The grains shown in Figure 8g,h appear to signify the Ti grain structure under the oxide film.

To illustrate the difference in the influence of the potential on the reactivity of the oxide on the grains and on the grain boundaries and triple points, Figure 9 shows the tip current along a line at $Y = 121.26$ μm at various substrate potentials shown in Figure 8. In reference to Figure 8, Figure 9 shows that point A is located over an oxide-covered grain, point B at the active spot believed to be a triple point, and point C, a new active area, possibly a grain boundary, which emerged as the potential applied to the Ti sample was made more

(70) Hua, F.; Mon, K.; Pasupathi, P.; Gordon, G.; Shoesmith, D. *Corrosion* **2005**, *61*, 987.

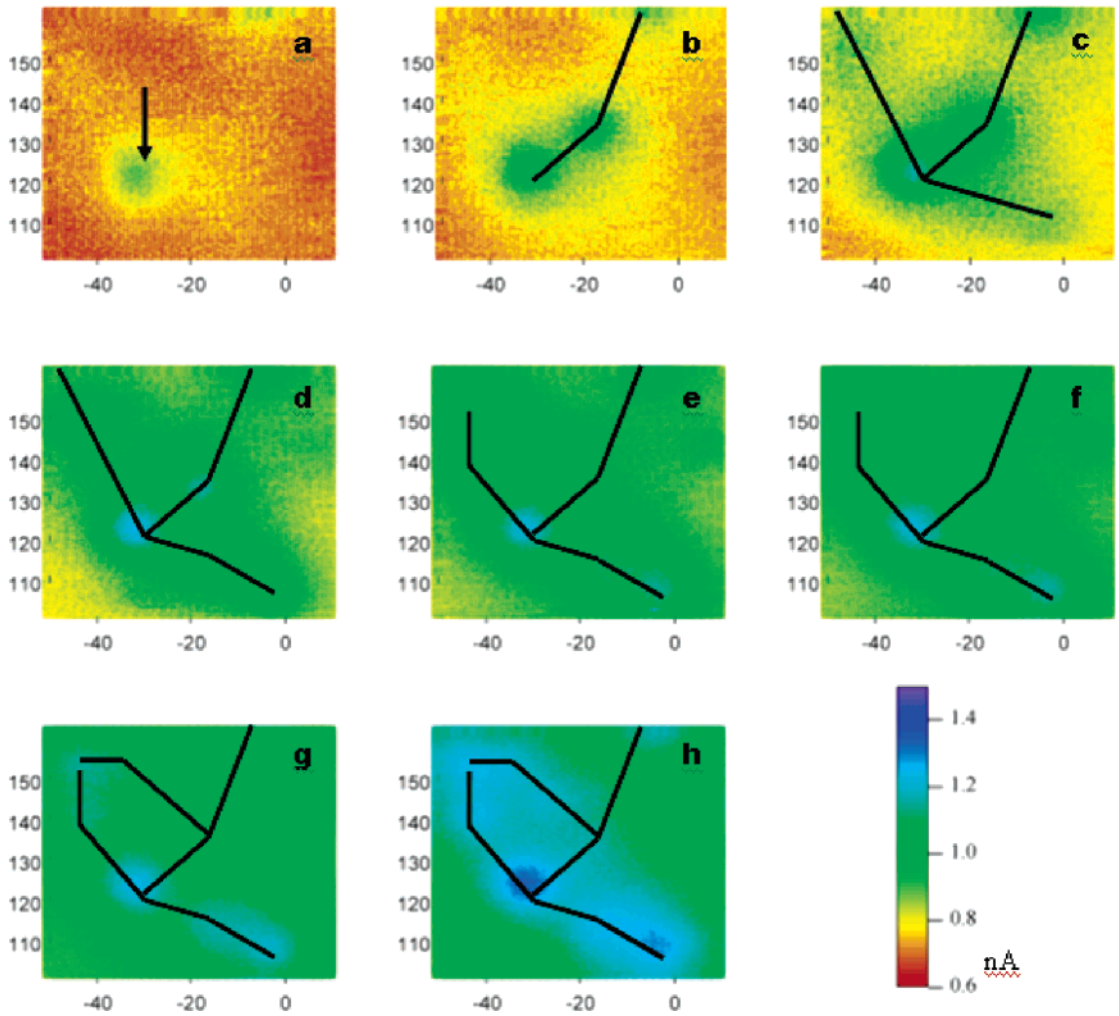

Figure 8. SECM images for the same Ti-2 area at various bias potentials. The imaged area was 60 μm × 60 μm, and one of the electrochemical reactive spots was centered. All the images have the same current scale, which is shown by the color bar (0.59−1.53 nA). The bias potentials on Ti-2 were (a) −0.05 V; (b) −0.10 V; (c) −0.15 V; (d) −0.20 V; (e) −0.25 V; (f) −0.30 V; (g) −0.35 V, and (h) −0.40 V. The distance between the tip and the Ti-2 sample was 3.0 μm. The active spot was labeled by the black arrow in image a. New active spots appeared on images b−h. These active spots can be connected by black lines to indicate grain boundaries. Other experimental conditions were the same as those described in Figure 6.

negative. These lines show that the current at all three locations increased with an increase in cathodic polarization, Figure 9b. However, the current at locations C and, especially, B increased more rapidly with decreasing potential than did the current at location A over the range −0.05 V to −0.20 V.

If the current at point A is attributed to the increased conductivity of the oxide due to its reduction and the absorption of H and the current at point B is attributed to the activity at a triple point, then it is clear that the triple point conductivity increased, independently of that of the oxide on the grain, at more positive potentials. The peak in the current difference (i(B) − i(A) in Figure 9b) indicates that the triple point became fully activated before the conversion of the oxide on the grain (via reaction 1) was complete. A similar, but less marked difference, between the current at point C and the current at point A was observed (i(C) − i(A) in Figure 9b), suggesting C may have been located at a grain boundary. This last suggestion is by no means certain, and it is possible that C was located on a grain covered by a thinner oxide than that at point A.[24,25]

It can be concluded from these results that the reductive transformation of the oxide on Ti begins at potentials much lower than previously claimed or calculated. Also, the oxides at the grain boundary structures and triple points are significantly less stable than the oxide on the grains. It is possible, therefore, that these locations could act as preferential entry windows for H absorption into the underlying Ti substrate.

PACs toward Different Spots on the Ti-2 Sample at Various Bias Potentials. Figure 10 shows the PACs recorded above two typical points on the Ti-2 surface at various bias potentials: one is an active spot (Figure 10a) and the other a nonactive spot (Figure 10b). When the bias potential on the Ti-2 sample was larger than 0.1 V, the surface was completely insulating, even at the active spot. Therefore, no positive feedback could be observed at this potential. The PACs for both the active and the nonactive sites overlapped with the theoretical curve for negative feedback very well. At this potential, the Ti oxide film is insulating, and electron transfer to Fc^+ does not occur.

When the potential was lower than 0.00 V, partial positive feedback was observed from the active spot (Figure 10a). As the potential was decreased further, positive feedback became more evident. The semiconducting TiO_2 energy barrier to charge transfer was lowered as the bands were bent in a favorable way to enrich the electrons at the

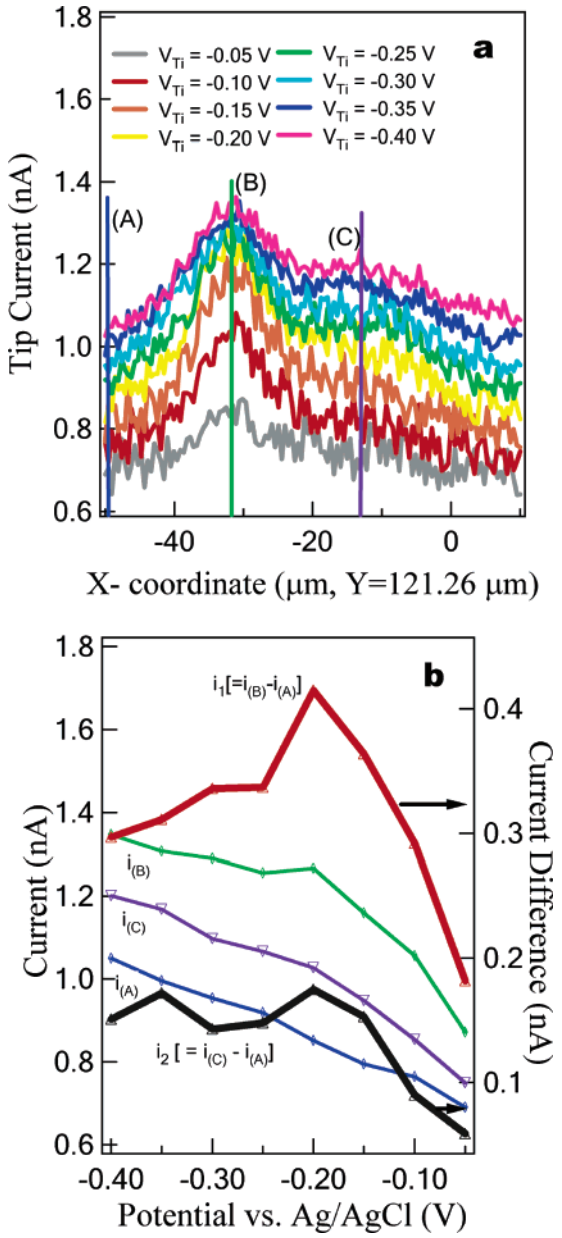

Figure 9. (a) Cross-section lines extracted from all the images in Figure 8 at $Y = 121.26$ μm (Y represents the vertical axis in the images). (b) Tip current changes versus the applied potential on the Ti-2 at the three spots where the coordinates are labeled in part a. The current difference between the triple point B and the nonactive point A (curve i_1) and that between the newly appearing active point C and the nonactive point A (curve i_2) are also plotted versus the bias potential on Ti-2 in (b).

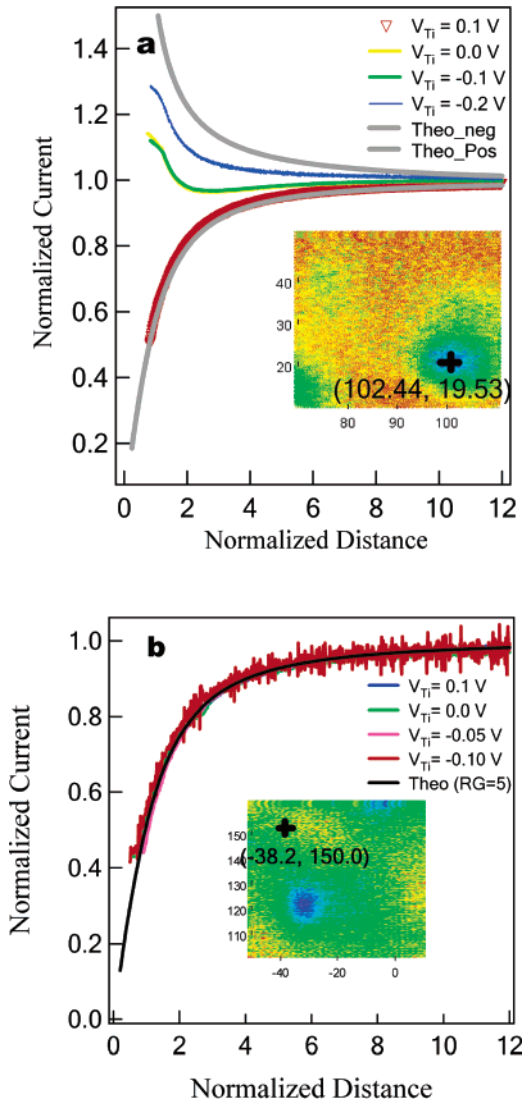

Figure 10. PACs recorded at an electroactive spot on Ti-2 at various applied potentials (a) and PACs recorded at a nonactive spot on Ti-2 at various applied potentials (b). The coordinates of both spots are labeled on the inserted SECM images (black cross). A potential of 0.4 V was applied to the CUME. The approach speed was 1.0 μm/s.

interface, thereby allowing Fc^+ reduction to Fc. This caused an increase in tip current, with positive feedback observed in the PACs.

Over the potential range of 0.20 V to −0.10 V, the PACs taken on the nonactive spots were all very similar and showed negative feedback. The negative feedback approach curves overlapped well with the theoretical curve for negative feedback (Figure 10b). While it is expected that partial positive feedback would be observed below −0.10 V, as mentioned above, we can conclude that, in the potential range 0.10 V to −0.10 V, the oxide film on the Ti-2 surface was very compact and stable. The oxide film does not favor the electron transfer to the ferrocenium, and the film is not reduced at potentials above −0.10 V.

CVs on the Tip at a Short Tip-to-Substrate Distance. The SECM tip was approached to the Ti-2 surface and stopped at a tip-to-substrate distance of 2.70 μm. Subsequently, the tip could be moved to either a nonactive spot or to an active site at the same height, respectively. At these two spots, CVs of the SECM probe were recorded while the bias potential on the Ti-2 was held at 0.0 and −0.10 V, respectively (Figure 11). This is the substrate generation-tip collection mode of SECM. The coordinates of the SECM probe are also shown in the inset images.

In bulk solution, where the tip was far away from the Ti-2 surface, the steady-state tip current was about 0.95 nA (CVs in red shown in Figure 11). At a height of 2.70 μm above the nonactive spot, the steady-state tip current was 0.47 nA when the bias potential on the Ti-2 was 0.00 V (CV in black, Figure 11a). This corresponds to 49% of the steady-state current in bulk solution and agrees very well with the theoretical PAC. With the same applied potential on the Ti-2, the steady-state current at a height of 2.70 μm above the active spot was 0.78 nA (CV in black, Figure 11b), 0.31 nA

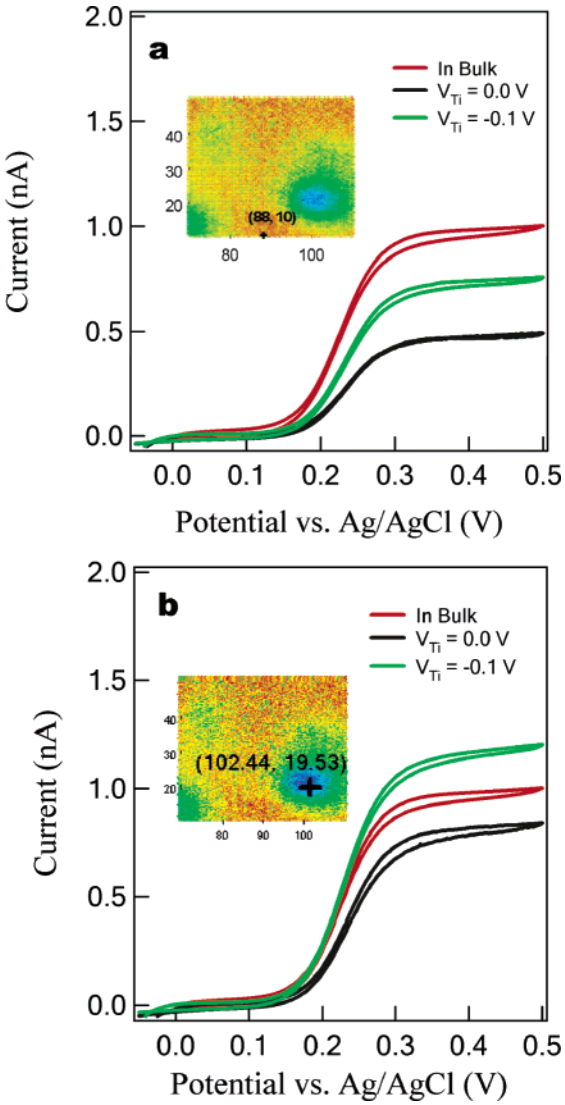

Figure 11. CVs recorded with the tip positioned above an electrochemically nonactive spot (a) and above an active spot (b). Both spots are labeled on the inserted SECM images (black crosses). The Ti-2 was biased at different potentials (0.00 V, the black line; −0.10 V, the green line; −0.20 V, the blue line). The tip-to-substrate distance was 3.2 μm. The potential limits on the tip were −0.05 to 0.50 V. The potential scan rate on the tip was 20 mV/s. The red CVs in both graphs were obtained when the tip was far away from the Ti-2 surface.

higher than the steady-state current obtained above the nonactive spot. This increased current value is a consequence of the partial positive feedback from this active spot. When the substrate potential was changed to −0.1 V, the steady-state current from the tip located above the active spot was 1.14 nA (CV in green, Figure 11b). This was 0.20 nA higher than when the tip was polarized in bulk solution and 0.43 nA higher than when the tip was located above the nonactive spot (0.71 nA as shown by CV in green, Figure 11a). Positive feedback was observed clearly at this potential. A more thorough investigation of such CVs on the Ti substrate is underway.

The quartile potential differences ($\Delta E_{1/4}$ and $\Delta E_{3/4}$) extracted from these CVs are listed in Table 2. At the same potential on Ti-2, the quartile potential differences of the tip from the active and nonactive spots are very similar. The feedback from the substrate did not affect the reaction property of the Fc redox reaction on the UME surface.

Table 2. Quartile Potentials and Their Differences Obtained from the CUME in Figure 11, Positioned above the Active and Nonactive Spots[a]

	active spot			non-active spot		
potential (V)	$E_{1/2}$ (mV)	$\Delta E_{1/4}$ (mV)	$\Delta E_{3/4}$ (mV)	$E_{1/2}$ (mV)	$\Delta E_{1/4}$ (mV)	$\Delta E_{3/4}$ (mV)
0.0	235	23	21	234	22	22
−0.1	228	23	22	232	21	22
bulk	225	28	29	225	28	29

[a] $\Delta E_{1/4} = E_{1/4} - E_{1/2}$ and $\Delta E_{3/4} = E_{1/2} - E_{3/4}$, where $E_{1/4}$ is the potential at the first fourth of the plateau current, $E_{1/2}$ is the potential at the second fourth of the plateau current, and so on.

Therefore, when the potential on the Ti-2 substrate was changed, the quartile potential differences were kept at a similar value. All these CVs showed that the Fc redox reaction on the CUME was reversible.[71]

Conclusions

SECM was used to determine the surface reactivity and grain boundary structures of a Ti-2 sample in 0.9 mM Fc solution. Because there were various microscale regions on the Ti-2 surface, a variety of different current feedback signals were obtained on the SECM tip. Therefore, the high current spots found on the SECM images, which we called "active spots", were related to the grain boundary and triple point structures in the material surface. Using these data, we constructed a grain boundary structure map on SECM images. This was further facilitated by imaging the Ti-2 at various applied potentials.

The surface reactivity was also assessed. The Ti-2 surface reactivity increased as the applied potential became more negative. As a result, more active spots were observed on the SECM images along the boundary structure at lower applied potentials.

Our claim that these spots are caused by the presence of Fe in the grain boundaries is supported by SEM/EDX analyses. Additional experiments with specimens containing various amounts of Fe are underway.

Further reactivity of the Ti substrate can be investigated by tip/substrate cyclic voltammetry at a short distance.

This noninvasive analytical method is by no means limited to Ti-2 and will find wide applications in materials science.

Acknowledgment. We appreciate the financial support from the Natural Science and Engineering Research Council of Canada (NSERC, New Discovery and Equipment Grants), Ontario Photonics Consortium (OPC), Canada Foundation for Innovation (CFI), Ontario Innovation Trust (OIT), the Premier's Research Excellence Award (PREA), and the University of Western Ontario (Academic Development Fund (ADF) and a Start-up Fund). Z.D. is grateful to the Swiss Federal Institute of Technology in Lausanne (EPFL) for a visiting professorship in Prof. Hubert H. Girault's group during the summer 2003. We thank Dr. Bernadette M. Quinn for her constructive discussions and suggestions on the fabrication of UMEs. We are thankful to Dr. J. Grauman (Timet, Hnderson, NV) for donating the Ti Grade-2 plate and Drs. Ian Mitchell, Xihua He, and Zack Qin, Mr. Yimin Zeng, and Ms. Li Yan for their kind help and discussion. Warren Lindsay, John Vanstone, Barakat

(71) Mirkin, M. V.; Richards, T. C.; Bard, A. J. *J. Phys. Chem.* **1993**, *97*, 7672.

Misk, Jon Aukema, Sherrie McPhee, Mary Lou Hart, and Marty Scheiring are gratefully acknowledged for their technical support. We would like to thank Dr. Todd Simpson and Ms. Nancy Bell of Nanofabrication Laboratory at UWO for their assistance in SEM.

Supporting Information Available: Detailed experimental procedures for CUME fabrication and characterization, PACs taken at active and nonactive spots on Ti-2 biased at 0.00 V versus Ag/AgCl, optical metallograph of the etched Ti-2, additional curves for the dependence on the substrate potential of the tip current difference between the active spot and the reference spot, additional SEM images, and EDX analysis (PDF). This material is available free of charge via the Internet at http://pubs.acs.org.

CM070023D